Available online at www.sciencedirect.com
SCIENCE DIRECT®
Journal of Power Sources 141 (2005) 359–368
JOURNAL OF POWER SOURCES
www.elsevier.com/locate/jpowsour

# Resistive companion modeling of batteries in a virtual test bed

Qi Zhang[a], Qingzhi Guo[a], Shengyi Liu[b], Roger A. Dougal[b], Ralph. E. White[a,*]

[a] *Center for Electrochemical Engineering, Department of Chemical Engineering, University of South Carolina, Columbia, SC 29208, USA*
[b] *Department of Electrical Engineering, University of South Carolina, Columbia, SC 29208, USA*

Received 12 September 2004; accepted 29 September 2004
Available online 8 December 2004

**Abstract**

The virtual test bed (VTB) computation environment provides an easy-to-use way for electric system modeling and simulation. Resistive companion (RC) modeling of batteries in VTB is presented in the paper. Native RC battery modeling approach and the one using current controlled voltage source (CCVS) interface are presented and compared through two battery models with different degrees of complexity. The RC battery models are validated by comparing VTB simulation data to those calculated directly through stand-alone Fortran codes. It is concluded that using CCVS interface is currently the first choice in modeling batteries in VTB. Simulations using the RC battery models in VTB are also presented and analyzed. It is shown that RC modeling provides a powerful way for the simulation of battery systems in VTB.


*Keywords:* Battery modeling; Resistive companion modeling; Current controlled voltage source; Virtual test bed

## 1. Introduction

In the last decade, the development of electric and hybrid vehicles and the rapid expansion of portable computers, consumer electronics and telecommunication tools in the world have spurred research into advanced battery systems with emphasis on operation under various conditions and on materials and cell construction to enhance cycle-life and performance. The research effort has been undertaken by both extensive experimental tests and computer simulations based on models evolved from physical and chemical laws of the processes occurring in the cell, i.e., first principles [1] or empirical models. These models play an important role in cell design in predicting cell performance under various conditions, and more recently, in the integration into electric system models [2,3] to highlight the real-time behaviors of the whole system. The latter feature is usually accomplished with circuit simulators, such as SPICE and virtual test bed (VTB) [2,4,5] developed at University of South Carolina.

The VTB software is dedicated to provide a unique capability for simulation and virtual prototyping of power electronic systems. The major modules of VTB software are schematic editor, visualization engine, system solvers and entities. VTB entities are the models of particular devices, i.e., resistor, capacitor and batteries, etc. They are coded in resistive companion (RC) [4–7] format which, by discretizing and linearizing time differential equations into algebraic equations, represents the physical circuit through a set of simultaneous algebraic equations analogous to those describe a direct current (dc) circuit. In the RC method, entities are connected to each other through ports or terminals. Each RC entity only handles its own governing equations. VTB system solvers collect the feedback from entities, that is, conductance matrices and current source vectors to generate system matrices and solve all interconnected devices in the system.

Batteries and fuel cells are important power sources in the electric system simulation. In the following, the paper

* Corresponding author. Tel.: +1 803 777 3270; fax: +1 803 777 9597.
*E-mail address:* white@engr.sc.edu (R.E. White).

0378-7753/$ – see front matter © 2004 Elsevier B.V. All rights reserved.
doi:10.1016/j.jpowsour.2004.09.023

**Nomenclature**

| | |
|---|---|
| $a$ | specific interfacial area in the cathode of the Li-ion battery ($m^2\ m^{-3}$) |
| $a_{neg}$ | specific surface area of negative electrode of the NiMH battery ($cm^2\ cm^{-3}$) |
| $a_{pos}$ | specific surface area of positive electrode of the NiMH battery ($cm^2\ cm^{-3}$) |
| $A_{neg}$ | geometry area of negative electrode of the NiMH battery ($cm^2\ cm^{-3}$) |
| $A_{pos}$ | geometry area of positive electrode of the NiMH battery ($cm^2\ cm^{-3}$) |
| $b$ | RC current source vector element |
| $B$ | RC current source vector |
| $c$ | concentration of electrolyte in the Li-ion battery ($mol\ m^{-3}$) |
| $c_e$ | concentration of KOH electrolyte in the NiMH battery ($mol\ cm^{-3}$) |
| $c_{max}$ | maximum Li salt concentration in polymer in the Li-ion battery ($mol\ m^{-3}$) |
| $c_{MH}$ | concentration of hydrogen in metal hydride in the NiMH battery ($mol\ cm^{-3}$) |
| $c_{Ni(OH)_2}$ | concentration of $Ni(OH)_2$ in the NiMH battery ($mol\ cm^{-3}$) |
| $c_s$ | concentration of lithium ions in the solid phase of the Li-ion battery ($mol\ m^{-3}$) |
| $c_{s,average}$ | average lithium ion concentration in an intercalation particle in the Li-ion battery ($mol\ m^{-3}$) |
| $c_T$ | maximum concentration of lithium ions in solid in the Li-ion battery ($mol\ m^{-3}$) |
| $D$ | diffusion coefficient of electrolyte in the polymer in the Li-ion battery ($m^2\ s^{-1}$) |
| $D_s$ | diffusion coefficient of lithium ion in the solid matrix in the Li-ion battery ($m^2\ s^{-1}$) |
| $E_0$ | open-circuit potential of the battery (V) |
| $f_\pm$ | mean activity coefficient of the electrolyte in the Li-ion battery |
| $F$ | faradic constant (98647 C equiv.$^{-1}$) |
| $g$ | RC conductance matrix element |
| $G$ | RC conductance matrix |
| $h$ | time step (s) |
| $i_{01}$ | exchange current density of anode reaction in the Li-ion battery ($A\ m^{-2}$) |
| $i_{0k}$ | exchange current density of reaction $k$ in the NiMH battery ($A\ cm^{-2}$) |
| $i_{cell}$ | applied current (A) |
| $i_k$ | current at node $k$ in the RC model (A) |
| $I$ | superficial current density in the Li-ion battery ($A\ m^{-2}$) |
| $j_n$ | pore wall flux of lithium ions ($mol\ m^{-2}\ s$) |
| $k_2$ | reaction rate constant at cathode/polymer interface in the Li-ion battery ($m^4\ mol^{-1}\ s^{-1}$) |
| $l_c$ | thickness of the cathode in the Li-ion battery (cm) |
| $l_{neg}$ | thickness of negative electrode in the NiMH battery (cm) |
| $l_{pos}$ | thickness of positive electrode in the NiMH battery (cm) |
| $l_s$ | thickness of the separator in the Li-ion battery (cm) |
| $l_{y,neg}$ | equivalent thickness of metal hydride material in the NiMH battery (cm) |
| $l_{y,pos}$ | equivalent thickness of nickel active material in the NiMH battery (cm) |
| $L_{MH}$ | loading of metal hydride material in the NiMH battery ($g\ cm^{-2}$) |
| $L_{Ni(OH)_2}$ | loading of nickel active material in the NiMH battery ($g\ cm^{-2}$) |
| $M_{MH}$ | molecular weight of metal hydride material($g\ mol^{-1}$) |
| $M_{Ni(OH)_2}$ | molecular weight of nickel active material ($g\ mol^{-1}$) |
| $n$ | number of electrons transferred in reactions in the Li-ion battery |
| $N_i$ | molar flux in $x$-direction of species $i$ in the Li-ion battery ($mol\ m^{-2}\ s$) |
| $p$ | gas pressure in the NiMH battery (atm) |
| $r$ | distance normal to surface of cathode material in the Li-ion battery (m) |
| $R$ | ideal gas constant ($8.3145\ J\ mol^{-1}\ K^{-1}$) |
| $R_{cell}$ | battery resistance ($\Omega$) |
| $R_s$ | radius of cathode material in the Li-ion battery (m) |
| $s_+$ | stoichiometric coefficient of Li ions in the Li-ion battery |
| SOC | state of charge in the NiMH battery |
| $t$ | independent time variable (s) |
| $t_+^0$ | transference number of lithium ions in the Li-ion battery |
| $T$ | temperature (K) |
| $U_{eq,i,ref}$ | equilibrium potential of reactions $i$ at reference reactant concentration in the NiMH battery (V) |
| $v_{cell}$ | close-circuit potential of the battery (V) |
| $v_k$ | node potential at node $k$ in the RC model (V) |
| $v_+$ | number of anions into which a mole of electrolyte dissociates in the Li-ion battery |
| $V_{gas}$ | gas volume in the NiMH battery ($cm^3$) |
| $V_{out}$ | output potential obtained in battery SFM model (V) |
| $x$ | spatial coordinate in the Li-ion battery (m) |
| $z_+$ | charge number of lithium ions in the Li-ion battery |

*Greek letters*

| | |
|---|---|
| $\Delta\phi_{neg}$ | potential difference at the solid and liquid interface on the negative electrode in the NiMH battery (V) |

| | |
|---|---|
| $\Delta\phi_{pos}$ | potential difference at the solid and liquid interface on the positive electrode in the NiMH battery (V) |
| $\varepsilon$ | porosity of electrode in the Li-ion battery |
| $\eta$ | cathode overpotential in the Li-ion battery (V) |
| $\kappa$ | conductivity of electrolyte in the Li-ion battery ($S\,m^{-1}$) |
| $\rho_{MH}$ | density of metal hydride active material in the NiMH battery ($g\,cm^{-3}$) |
| $\rho_{Ni(OH)_2}$ | density of nickel active material in the NiMH battery ($g\,cm^{-3}$) |
| $\sigma$ | conductivity of sold matrix in the Li-ion battery ($S\,m^{-1}$) |
| $\Phi_1$ | solid phase potential in the Li-ion battery (V) |
| $\Phi_2$ | liquid phase potential in the Li-ion battery (V) |
| *Superscript* | |
| 0 | initial condition |

presents and compares RC battery modeling methods which evolve with the complexity of battery models.

## 2. Resistive companion modeling of batteries

### 2.1. Overview

A simple battery model as described by Eq. (1) is referred to explain RC battery modeling:

$$v_{cell} = E_0 + i_{cell} R_{cell} \tag{1}$$

where $v_{cell}$ is the close-circuit potential, $E_0$ the open-circuit potential, $i_{cell}$ the applied current, and $R_{cell}$ the internal resistance of the battery. In Eq. (1), it is assumed that the battery has a constant open-circuit potential and close-circuit potential varies linearly with applied current. Such a battery is often viewed as a voltage source with internal resistance. However, resistive companion method requires all entities to be represented as current source and resistance parallel combinations [5]. The battery needs to be replaced with an equivalent circuit consisting of the parallel combination of a resistor and current source by applying Thevenin–Norton transformation [6] (see Fig. 1). The close circuit voltage $v_{cell}$ and applied current $i_{cell}$ can be related to terminal potential and current variables by

$$v_{cell} = v_0 - v_1 \tag{2}$$

$$i_{cell} = i_0 = -i_1 \tag{3}$$

where $v_0$, $v_1$ are node potentials and $i_0$, $i_1$ the node currents.

For an electric device with two terminals, the resistive companion method expects the following relation:

$$I(t) = G(t-h)V(t) - B(t-h) \tag{4}$$

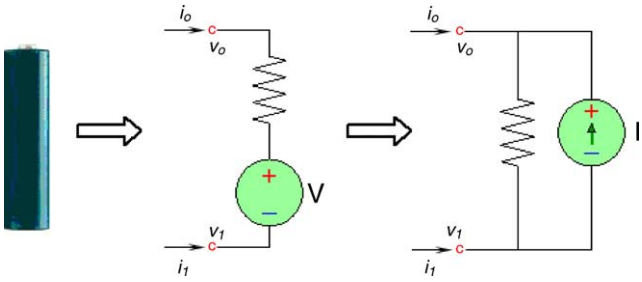


Fig. 1. Battery RC model with Thevenin–Norton transformation.

where the conductance matrix is of the form $G(t-h) = \begin{bmatrix} g_{00} & g_{01} \\ g_{10} & g_{11} \end{bmatrix}$, the current source vector of the form $B(t-h) = \begin{bmatrix} b_0 \\ b_1 \end{bmatrix}$, $t$ the time and $h$ the time step. The conductance matrix elements are given by

$$g_{jk}(t-h) = \left(\frac{\partial i_j}{\partial v_k}\right)_{t-h}, \quad \text{where} \quad j,k = 0,1 \tag{5}$$

and current source vector elements are given by

$$b_j(t-h) = -i_j(t-h) + \sum_k g_{jk} v_k(t-h), \quad \text{where} \quad j,k = 0,1 \tag{6}$$

From Eqs. (1)–(6), we can obtain the RC representation for the battery:

$$\begin{bmatrix} i_0(t) \\ i_1(t) \end{bmatrix} = \begin{bmatrix} \frac{1}{R_{cell}} & -\frac{1}{R_{cell}} \\ -\frac{1}{R_{cell}} & \frac{1}{R_{cell}} \end{bmatrix} \begin{bmatrix} v_0(t) \\ v_1(t) \end{bmatrix} - \begin{bmatrix} \frac{E_0}{R_{cell}} \\ -\frac{E_0}{R_{cell}} \end{bmatrix} \tag{7}$$

The conductance matrix and current source vector are used by VTB solvers in the numerical calculations. If the battery has fixed open-circuit potential $E_0$ and internal resistance $R_{cell}$ which is the case in Eq. (1), the elements of its conductance matrix and current source vector are all constants. Devices of such kind are called *linear* entities [5] in VTB. However, the battery model (Eq. (1)) is oversimplified, i.e. it does not reflect the change of the open-circuit potential with the state of charge (SOC) and the battery internal resistance may also vary in the process of discharge. Many battery models available in the literature are more sophisticated than Eq. (1) and are usually represented by a set of nonlinear algebraic-differential equations yielding *nonlinear* entities [5] in VTB environment. In the following sections, two battery models with different complexity chosen from the literature are discussed in details as extensions of the RC battery modeling in VTB environment.

### 2.2. Native RC modeling of a nickel metal hydride (NiMH) cell

A nickel metal hydride cell model described by Wu et al. [7] is used here to introduce native RC modeling of batteries

of which the open-circuit potential varies with the SOC. It is assumed in the model that both the positive and negative electrodes are planar electrodes and diffusion process inside the solid active material is not important. Four reactions in the nickel metal hydride cell have been considered. They are:

- Nickel electrode

$$\mathrm{NiOOH + H_2O + e^- \underset{\text{charge}}{\overset{\text{discharge}}{\rightleftarrows}} Ni(OH)_2 + OH^-} \tag{8}$$

$$2\mathrm{OH^-} \rightarrow \frac{1}{2}\mathrm{O_2 + H_2O + 2e^-} \tag{9}$$

- Metal hydride electrode

$$\mathrm{MH + OH^- \underset{\text{charge}}{\overset{\text{discharge}}{\rightleftarrows}} H_2O + M + e^-} \tag{10}$$

$$\frac{1}{2}\mathrm{O_2 + H_2O + 2e^- \rightarrow 2OH^-} \tag{11}$$

The governing equations for the cell are:

$$l_{y,\mathrm{pos}}\frac{\mathrm{d}c_{\mathrm{Ni(OH)_2}}}{\mathrm{d}t} = -\frac{j_1}{F} \tag{12}$$

$$l_{y,\mathrm{neg}}\frac{\mathrm{d}c_{\mathrm{MH}}}{\mathrm{d}t} = -\frac{j_3}{F} \tag{13}$$

$$\frac{V_{\mathrm{gas}}}{RT}\frac{\mathrm{d}p_{\mathrm{O_2}}}{\mathrm{d}t} = \frac{a_{\mathrm{pos}}l_{\mathrm{pos}}A_{\mathrm{pos}}j_2 + a_{\mathrm{neg}}l_{\mathrm{neg}}A_{\mathrm{neg}}j_4}{F} \tag{14}$$

$$i_{\mathrm{cell}} = a_{\mathrm{pos}}l_{\mathrm{pos}}A_{\mathrm{pos}}(j_1 + j_2) \tag{15}$$

$$-i_{\mathrm{cell}} = a_{\mathrm{neg}}l_{\mathrm{neg}}A_{\mathrm{neg}}(j_3 + j_4) \tag{16}$$

$$v_{\mathrm{cell}} = (\Delta\phi_{\mathrm{pos}} - \Delta\phi_{\mathrm{neg}}) + i_{\mathrm{cell}}R_{\mathrm{cell}} \tag{17}$$

where

$$j_1 = i_{01}\left[\begin{array}{l}\left(\dfrac{c_{\mathrm{Ni(OH)_2}}}{c_{\mathrm{Ni(OH)_2,ref}}}\right)\left(\dfrac{c_{\mathrm{e}}}{c_{\mathrm{e,ref}}}\right) \\ \quad\times\exp\left(\dfrac{0.5F}{RT}(\Delta\phi_{\mathrm{pos}} - U_{\mathrm{eq,1,ref}})\right) \\ -\left(1 - \dfrac{c_{\mathrm{Ni(OH)_2}}}{c_{\mathrm{Ni(OH)_2,ref}}}\right) \\ \quad\times\exp\left(-\dfrac{0.5F}{RT}(\Delta\phi_{\mathrm{pos}} - U_{\mathrm{eq,1,ref}})\right)\end{array}\right] \tag{18}$$

$$j_2 = i_{02}\left[\begin{array}{l}\left(\frac{c_{\mathrm{e}}}{c_{\mathrm{e,ref}}}\right)^2\exp\left(\dfrac{F}{RT}(\Delta\phi_{\mathrm{pos}} - U_{\mathrm{eq,2,ref}})\right) \\ -\left(\dfrac{p_{\mathrm{O_2}}}{p_{\mathrm{O_2,ref}}}\right)^{0.5} \\ \quad\times\exp\left(-\dfrac{F}{RT}(\Delta\phi_{\mathrm{pos}} - U_{\mathrm{eq,2,ref}})\right)\end{array}\right] \tag{19}$$

$$j_3 = i_{03}\left[\begin{array}{l}\left(\dfrac{c_{\mathrm{MH}}}{c_{\mathrm{MH,ref}}}\right)\left(\dfrac{c_{\mathrm{e}}}{c_{\mathrm{e,ref}}}\right)\exp\left(\dfrac{0.5F}{RT}(\Delta\phi_{\mathrm{neg}} - U_{\mathrm{eq,3,ref}})\right) \\ -\exp\left(-\dfrac{0.5F}{RT}(\Delta\phi_{\mathrm{neg}} - U_{\mathrm{eq,3,ref}})\right)\end{array}\right] \tag{20}$$

$$j_4 = -\frac{p_{\mathrm{O_2}}}{p_{\mathrm{O_2,ref}}}i_{4,\mathrm{ref}} \tag{21}$$

$$l_{y,\mathrm{pos}} = \frac{L_{\mathrm{Ni(OH)_2}}}{\rho_{\mathrm{Ni(OH)_2}}l_{\mathrm{pos}}a_{\mathrm{pos}}} \tag{22}$$

$$l_{y,\mathrm{neg}} = \frac{L_{\mathrm{MH}}}{\rho_{\mathrm{MH}}l_{\mathrm{pos}}a_{\mathrm{pos}}} \tag{23}$$

The initial conditions for Eqs. (12)–(14) are:

$$\frac{c^0_{\mathrm{Ni(OH)_2}}}{c_{\mathrm{Ni(OH)_2,max}}} = 1 - \mathrm{SOC}^0 \tag{24}$$

$$\frac{c^0_{\mathrm{MH}}}{c_{\mathrm{MH,max}}} = \mathrm{SOC}^0\frac{L_{\mathrm{Ni(OH)_2}}A_{\mathrm{pos}}M_{\mathrm{MH}}}{L_{\mathrm{MH}}A_{\mathrm{neg}}M_{\mathrm{Ni(OH)_2}}} \tag{25}$$

$$p^0_{\mathrm{O_2}} = 0.1\,\mathrm{atm} \tag{26}$$

Eqs. (12)–(17) need to be converted to RC format by discretizing equations within one time step and calculating the conductance matrix and current source vector using Eqs. (5) and (6). As seen in Eqs. (12)–(17), the model equations are nonlinear with respect to the variables such as $\Delta\phi_{\mathrm{pos}}$, $c_{\mathrm{Ni(OH)_2}}$,$c_{\mathrm{MH}}$, and $\Delta\phi_{\mathrm{neg}}$. Analytical solutions for the RC matrices are not available. One common practice is to use finite difference approximation to calculate the RC matrices numerically:

$$\begin{aligned} g_{jk} &= \left(\frac{\partial i_j}{\partial v_k}\right)_{t-h} = (-1)^{j+k}\frac{\mathrm{d}i_{\mathrm{cell}}}{\mathrm{d}v_{\mathrm{cell}}} \\ &= (-1)^{j+k}\frac{i_{\mathrm{cell}} + \Delta i - i_{\mathrm{cell}}}{v_{\mathrm{cell}} + \Delta v - v_{\mathrm{cell}}}, \quad \text{where } j,k = 0,1 \end{aligned} \tag{27}$$

$$\begin{aligned} b_j &= -i_j + \sum_k g_{jk}v_k = (-1)^j\left(\frac{\mathrm{d}i_{\mathrm{cell}}}{\mathrm{d}v_{\mathrm{cell}}}v_{\mathrm{cell}} - i_{\mathrm{cell}}\right) \\ &= (-1)^j\left(\frac{i_{\mathrm{cell}} + \Delta i - i_{\mathrm{cell}}}{v_{\mathrm{cell}} + \Delta v - v_{\mathrm{cell}}}v_{\mathrm{cell}} - i_{\mathrm{cell}}\right), \\ &\quad \text{where } j,k = 0,1 \end{aligned} \tag{28}$$

The perturbation of the cell voltage ($\Delta v$) or cell current ($\Delta I$) must be small enough to provide good numerical accuracy for the RC matrices. A Fortran solver call GNES is used to provide model solutions numerically.

### 2.3. RC modeling of a Li-ion cell

First principle battery models are built on our understanding of the battery physics, including the microscopic

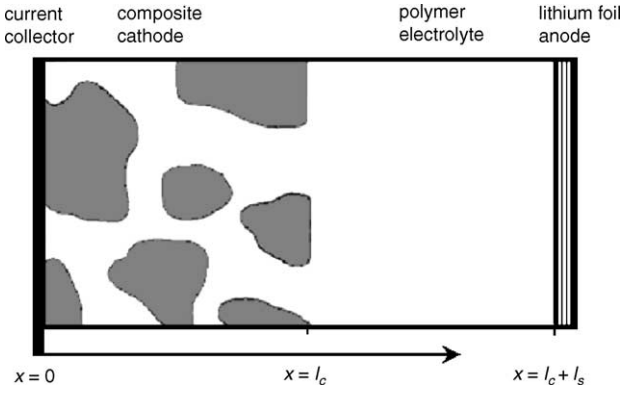


Fig. 2. Lithium/polymer cell sandwich.

electrode reactions and transport phenomena inside the porous electrodes. Some first principle models further incorporate coupled electrochemical and thermal behaviors to reflect the thermal influence on the performance of the battery. They are more rigorous in describing battery behaviors, but are more complicated. A first principle battery model described by Doyle et al. [8] is presented to illustrate how to model such complicated batteries through RC method in VTB environment.

Doyle et al. [8] used the model to simulate the galvanostatic charge/discharge behavior of the cell sandwich shown in Fig. 2. The model considers one-dimensional transport of lithium ion from the lithium anode through the polymer separator into the composite cathode. The reaction at the anode is assumed to take the form:

$$\mathrm{Li} + \Theta_\mathrm{p} \rightleftarrows \mathrm{Li}^+ - \Theta_\mathrm{p} + \mathrm{e}^- \tag{29}$$

And the reaction at the cathode is assumed to take the form:

$$\mathrm{Li}^+ - \Theta_\mathrm{p} + \Theta_\mathrm{s} + \mathrm{e}^- \rightleftarrows \mathrm{Li}^+ - \Theta_\mathrm{s} + \Theta_\mathrm{p} \tag{30}$$

The governing equations for the Li-ion battery are:

- at the anode:

$$I = i_{01}\left[\exp\left(\frac{0.5F(\Phi_1|_{x=l_\mathrm{c}+l_\mathrm{s}} - \Phi_2|_{x=l_\mathrm{c}+l_\mathrm{s}})}{RT}\right) - \exp\left(-\frac{0.5F(\Phi_1|_{x=l_\mathrm{c}+l_\mathrm{s}} - \Phi_2|_{x=l_\mathrm{c}+l_\mathrm{s}})}{RT}\right)\right] \tag{31}$$

- in the separator:

$$\frac{\partial c}{\partial t} = D\frac{\partial^2 c}{\partial x^2} - \frac{I}{z_+\nu_+F}\frac{\partial t_+^0}{\partial x} \tag{32}$$

$$I = -\kappa\frac{\partial \Phi_2}{\partial x} - \frac{\kappa RT}{F}\left(\frac{s_+}{n\nu_+} + \frac{t_+^0}{z_+\nu_+}\right)\frac{\partial \ln c}{\partial x} \tag{33}$$

- in the composite cathode:

$$\varepsilon\frac{\partial c}{\partial t} = \varepsilon^{1.5}D\frac{\partial^2 c}{\partial x^2} - \frac{I + \sigma(\partial\Phi_1/\partial x)}{z_+\nu_+F}\frac{\partial t_+^0}{\partial x} + \frac{aj_n(1-t_+^0)}{\nu_+} \tag{34}$$

$$\frac{\partial(\eta - \Phi_1)}{\partial x} = \frac{I}{\kappa} + \frac{\sigma}{\kappa}\frac{\partial \Phi_1}{\partial x} + \frac{RT}{F}\left(\frac{s_+}{n\nu_+} + \frac{t_+^0}{z_+\nu_+}\right)\frac{\partial \ln c}{\partial x} \tag{35}$$

$$aj_n = \frac{s_+}{nF}\sigma\frac{\partial^2\Phi_1}{\partial x^2} \tag{36}$$

$$j_n = k_2(c_\mathrm{max} - c)^{0.5}c^{0.5} \times \begin{bmatrix} c_\mathrm{s}|_{r=R_\mathrm{s}}\exp\left(\frac{0.5F}{RT}(\eta - U')\right) \\ -(c_\mathrm{T} - c_\mathrm{s}|_{r=R_\mathrm{s}})\exp\left(-\frac{0.5F}{RT}(\eta - U')\right) \end{bmatrix} \tag{37}$$

$$\frac{\partial c_\mathrm{s}}{\partial t} = D_\mathrm{s}\left[\frac{\partial^2 c_\mathrm{s}}{\partial r^2} + \frac{2}{r}\frac{\partial c_\mathrm{s}}{\partial r}\right] \tag{38}$$

- with the boundary conditions:

$$\left(-D\frac{\partial c}{\partial x} + It_+^0\right)|_{x=l_\mathrm{c}+l_\mathrm{s}} = \frac{I}{F} \tag{39}$$

$$\frac{\partial c}{\partial x}|_{x=0} = 0 \tag{40}$$

$$\frac{\partial c_\mathrm{s}}{\partial r}|_{r=0} = 0 \tag{41}$$

$$j_n = -D_\mathrm{s}\frac{\partial c_\mathrm{s}}{\partial r}|_{r=R_\mathrm{s}} \tag{42}$$

$$\frac{\partial \Phi_1}{\partial x}|_{x=0} = -\frac{I}{\sigma} \tag{43}$$

$$\frac{\partial \Phi_1}{\partial x}|_{x=l_\mathrm{c}-} = 0 \tag{44}$$

and the battery close circuit voltage is defined as

$$v_\mathrm{cell} = \Phi_1|_{x=0} - \Phi_1|_{x=l_\mathrm{c}+l_\mathrm{s}} \tag{45}$$

The equations mentioned above to model the Li-ion cell is computation intensive because the solutions for both *x*-direction and *r*-direction need to be obtained. Venkat's approximation [9] is applied to eliminate the need to solve Eq. (38) in *r*-direction by converting the equation to two differential and algebraic equations:

$$\frac{\partial c_\mathrm{s,average}}{\partial t} + \frac{15D_\mathrm{s}}{R_\mathrm{s}^2}(c_\mathrm{s,average} - c_\mathrm{s}|_{r=R_\mathrm{s}}) = 0 \tag{46}$$

$$j_n = \frac{5D_\mathrm{s}}{R_\mathrm{s}}(c_\mathrm{s,average} - c_\mathrm{s}|_{r=R_\mathrm{s}}) \tag{47}$$

To solve the model equations, finite difference approximation is used to discretize the special coordinate *x*. Hundred internal node points are used to achieve good convergence and desired accuracy. After discretization, the total number of equations is close to $10^3$. A Standard Fortran solver called DASSL is used to provide numerical solution. If the Li-ion battery is modeled in the native RC method, the RC model is a nonlinear entity in VTB and must be called several times

in each time step in order for system to converge upon a solution at time $t$ [5]. And in each call, model equations have to be solved twice to get battery resistance. Therefore, the native RC modeling method is not expected to be efficient in dealing with such batteries where the number of battery model equations is large, i.e., $10^3$. It is desired that a new RC modeling method could be used to achieve higher numerical efficiency than the native one.

It should be noticed that the close circuit voltage obtained through Eq. (45) in the Li-ion battery model is actually decoupled from the rest of governing equations if the charge/discharge current is selected as the control variable in solving the discretized model equations. In such case, there exists a sparse Jacobian matrix and numerical efficiency can be greatly improved by taking advantage of the banded structure of the Jacobian matrix [10]. However, if the voltage is selected as the control variable, Eq. (45) must be coupled to the rest of model equation to solve the model and the computation time will be great due to the un-banded structure of the Jacobian matrix. Hence it would be much better that the new modeling method could exploit the decoupled feature of the cell voltage equation in solving the battery model.

Such a RC modeling method using current controlled voltage source (CCVS) interface is brought forward by the Department of Electrical Engineering at the University of South Carolina. The method was originally used to interface VTB simulator with the ACSL (advanced circuit simulation language) based models [11]. Before it is introduced, some related background information is provided.

VTB simulator uses resistive companion method while other simulators such as ACSL use signal flow method (SFM). When the battery model is solved with a Fortran solver like DASSL, it acts like a SFM model. For example, with some input of applied current ($I_{\text{in}}$), the battery model can calculate close circuit potential ($V_{\text{out}}$) and other state variables reflecting battery conditions as output (see Fig. 3). An interface or wrapper has to be used if one wants to connect VTB RC model and SFM models together.

The CCVS interface [11] used to connect ACSL and VTB is adapted in the new RC battery modeling method. The interface implements natural coupling which requires enforcement of physical conservation principles to connect the SFM battery model with the RC battery model (VTB entity) (see Fig. 4).

The RC format for the CCVS interface is formulated using modified node analysis [6]:

$$\begin{bmatrix} i_0(t) \\ i_1(t) \\ 0 \end{bmatrix} = \begin{bmatrix} 0 & 0 & 1 \\ 0 & 0 & -1 \\ 1 & -1 & 0 \end{bmatrix} \begin{bmatrix} v_0(t) \\ v_1(t) \\ I(t) \end{bmatrix} - \begin{bmatrix} 0 \\ 0 \\ V_{\text{out}} \end{bmatrix} \tag{48}$$

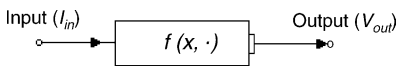


Fig. 3. Schematic of SFM type battery models.

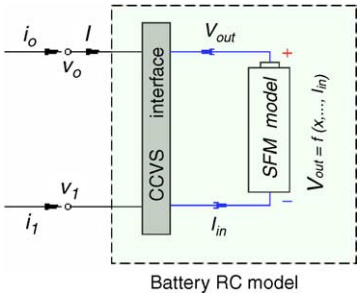


Fig. 4. Battery RC model with CCVS interface. $I$ is branch current and $I_{\text{in}} = I$.

Comparing to the native modeling method, a branch current $I$ is introduced as an additional variable and the conductance matrix $G = \begin{bmatrix} 0 & 0 & 1 \\ 0 & 0 & -1 \\ 1 & -1 & 0 \end{bmatrix}$ and current source vector $B = \begin{bmatrix} 0 \\ 0 \\ V_{\text{out}} \end{bmatrix}$ are augmented to reflect the change. The algorithm works in the following way. The RC battery model obtains the known values of node voltage $v_0$, $v_1$ and branch current $I$ at time step $t' = t$ from the system solver and passes the branch current to the SFM battery model which returns the close circuit voltage $V_{\text{out}}$ as output. Then the RC battery model assembles the RC matrices and returns them to the RC system solver to determine new values of node voltage $v_0$, $v_1$ and branch current $I$ at time step $t' = t + h$.

Connected through the interface, the battery SFM model appears as a current controlled voltage source (CCVS) which is a linear entity in the VTB system. Consequently, the system matrices are not susceptible to any nonlinearity wrapped inside the SFM models and modelers can select appropriate solvers for the SFM models without affecting VTB system solvers. And most importantly, the battery SFM model needs to be solved only once in each time step due to the feature of linear VTB entity, which is critical in speeding up the simulation.

## 3. Model validation and simulations

The VTB RC models are required to be coded in C language and implemented as dynamic link libraries (DLLs). A DLL is an executable file that acts as a shared library of functions with imports and exports. But it is more efficient to code the battery SFM models in Fortran than in C because of the huge body of robust Fortran numerical algorithms available in public domain, such as the standard DASSL subroutine for differential-algebraic equations. The battery SFM models used in this paper are also implemented as DLLs. Such modular structure can be easily debugged separately and adapted to other battery models. In order for battery SFM model (Fortran DLL) to correctly communicate with the CCVS interface and RC model (C DLL), mixed language programming [12]

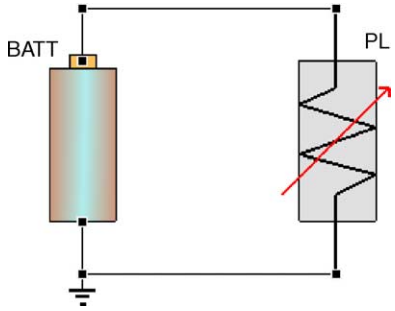


Fig. 5. Simulation schematic used in model validation.

is required. The calling convention of SFM model (Fortran DLL) has to match that of RC model (C DLL) and the arguments type of Fortran subroutine must be correctly declared in the caller RC model. Both DLLs must be provided to VTB to make battery models work in VTB environment.

The validity of the RC battery models is evaluated using following simulation schematic (see Fig. 5). The PL in the figure is a programmable load. Two options are used in the validation: battery discharging with constant current load and resistance load. RC NiMH battery models and RC Li-ion battery models using both native modeling method and the one with CCVS interface are validated in the simulation. The parameters for the battery models are listed in Tables 1 and 2,

Table 1
Parameters for the NiMH battery model

| Parameter | Value |
|---|---|
| $a_{pos}$ ($cm^2\ cm^{-3}$) | 4000.0 |
| $a_{neg}$ ($cm^2\ cm^{-3}$) | 1000.0 |
| $A_{pos}$ ($cm^2$) | 325.0 |
| $A_{neg}$ ($cm^2$) | 360.0 |
| $c_e$ ($mol\ cm^{-3}$) | $7.0 \times 10^{-3}$ |
| $c_{e,ref}$ ($mol\ cm^{-3}$) | $1.0 \times 10^{-3}$ |
| $c_{MH,max}$ ($mol\ cm^{-3}$) | $1.0 \times 10^{-1}$ |
| $c_{MH,ref}$ ($mol\ cm^{-3}$) | 0.5 |
| $c_{Ni(OH)_2,max}$ ($mol\ cm^{-3}$) | $3.7 \times 10^{-2}$ |
| $c_{Ni(OH)_2,ref}$ ($mol\ cm^{-3}$) | 0.5 |
| $i_{01}$ ($A\ cm^{-2}$) | $1.0 \times 10^{-4}$ |
| $i_{02}$ ($A\ cm^{-2}$) | $1.0 \times 10^{-10}$ |
| $i_{03}$ ($A\ cm^{-2}$) | $3.8 \times 10^{-4}$ |
| $i_{04}$ ($A\ cm^{-2}$) | $1.0 \times 10^{-4}$ |
| $l_{pos}$ (cm) | $3.3 \times 10^{-2}$ |
| $l_{neg}$ (cm) | $2.8 \times 10^{-2}$ |
| $L_{Ni(OH)_2}$ ($g\ cm^{-2}$) | $6.8 \times 10^{-2}$ |
| $L_{MH}$ ($g\ cm^{-2}$) | $1.13 \times 10^{-1}$ |
| $M_{Ni(OH)_2}$ ($g\ mol^{-1}$) | 92.71 |
| $M_{MH}$ ($g\ mol^{-1}$) | 70.58 |
| $p_{O_2,ref}$ (atm) | 1.0 |
| $R_{cell}$ (Ω) | $1.0 \times 10^{-3}$ |
| $SOC^0$ | 0.95 |
| $T$ (K) | 298.15 |
| $U_{eq,1,ref}$ (V) | 0.527 |
| $U_{eq,2,ref}$ (V) | 0.4011 |
| $U_{eq,3,ref}$ (V) | −0.8279 |
| $V_{gas}$ ($cm^3$) | 1.01 |
| $\rho_{Ni(OH)_2}$ ($g\ cm^{-3}$) | 3.4 |
| $\rho_{MH}$ ($g\ cm^{-3}$) | 7.49 |

Table 2
Parameters for the Li-ion battery model

| Parameter | Value |
|---|---|
| $a$ ($m^2$) | 1.0 |
| $c_{max}$ ($mol\ m^{-3}$) | 3920.0 |
| $c_T$ ($mol\ m^{-3}$) | 29000.0 |
| $D$ ($m^2\ s^{-1}$) | $7.5 \times 10^{-12}$ |
| $D_s$ ($m^2\ s^{-1}$) | $5.0 \times 10^{-13}$ |
| $i_{01}$ ($A\ m^{-2}$) | 12.6 |
| $k_2$ ($m^4\ s^{-1}\ mol$) | $1.0 \times 10^{-10}$ |
| $l_c$ (m) | $100.0 \times 10^{-6}$ |
| $l_s$ (m) | $50.0 \times 10^{-6}$ |
| $n$ | 1.0 |
| $R_s$ (m) | $1.0 \times 10^{-6}$ |
| $T$ (K) | 373.2 |
| $\nu_+$ | 1.0 |
| $\varepsilon$ | 0.3 |
| $\sigma$ ($S\ m^{-1}$) | $1.0 \times 10^4$ |
| $\kappa$ ($S\ m^{-1}$) | 2.176 |

respectively. The VTB simulation results are compared with those obtained by solving system (Fig. 5) integratedly with stand-alone Fortran codes.

Simulation results are presented in Figs. 6–9. The differences among the results obtained through three methods are nearly indistinguishable as the plots show, where the lines are overlapped. However, there is a great discrepancy in the computation time used in the simulation as shown in Table 3.

It can be seen from Table 3 that solving the system with stand-alone Fortran codes is faster than using either RC models. But such an advantage is outweighed by the disadvantage of the need to re-program the Fortran codes when the simulated system changes. It is impossible for a stand-alone Fortran code to consider all possible combinations of large variant models which may be used in the simulation. Modeling and simulation in VTB allows for reuse of existing codes (entities) and complex system simulation can be more easily conducted. It is apparent that battery RC models in CCVS interface can run more efficiently and obtain fairly accurate

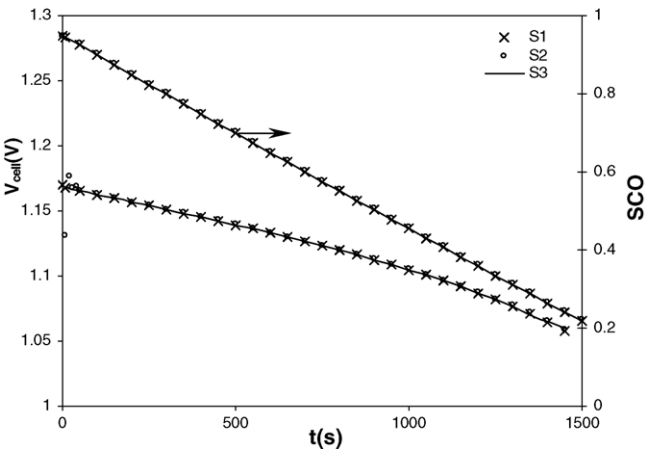


Fig. 6. Simulation run 1: NiMH battery discharge with constant resistance load of 0.1 Ω. S1 is obtained using native RC battery model, S2, using CCVS interface model and S3 using stand-alone Fortran code.

Table 3
Highlights of simulation results

| | | NiMH battery model | | | Li-ion battery model | | |
|---|---|---|---|---|---|---|---|
| | | S1 | S2[a] | S3 | S1 | S2[a] | S3 |
| Percentage error[b] ($V_{cell}$) | Run 1 | <0.005 | <0.01 | N/A | <0.1 | <0.1 | N/A |
| | Run 2 | <0.005 | <0.01 | N/A | <0.01 | <0.05 | N/A |
| Simulation time[c] (s) | Run 1 | ∼1.2 | ∼0.4 | ∼0.2 | >100 | ∼4 | ∼1.2 |
| | Run 2 | ∼1.2 | ∼0.4 | ∼0.2 | >100 | ∼0.4 | ∼0.2 |

[a] Data which have not converged are excluded from calculating the percentage error.
[b] The percentage errors are calculated by comparing the cell voltage data simulated by the RC models to the data simulated by the stand-alone Fortran codes.
[c] Simulation time is based on 1000 step.

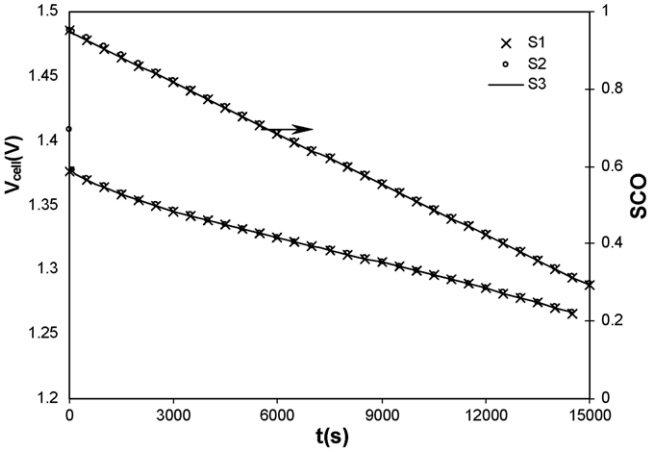


Fig. 7. Simulation run 2: NiMH battery discharge with constant current load of 1 A. See Fig. 6 for the meaning of the legend.

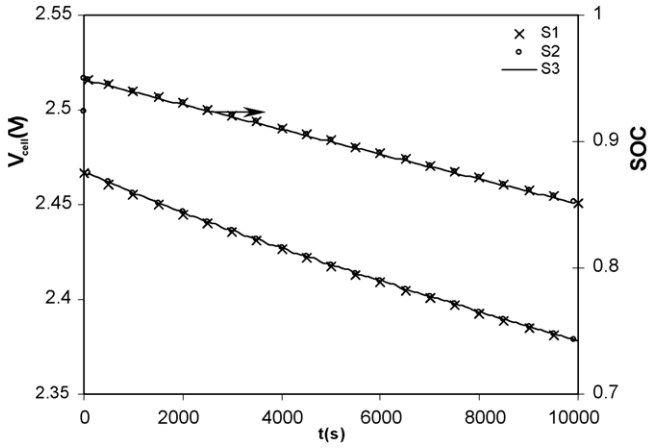


Fig. 9. Simulation run 2: Li-ion battery discharge with constant current load of 2 A. See Fig. 6 for the meaning of the legend.

results as compared with those modeled in native RC method. The computation time saved from the linear feature of RC model with CCVS interface is significant when the number of model equations is very large. Therefore, it is concluded from our work that using the CCVS interface currently should be the first choice in RC battery modeling in VTB environment, especially in the case where a battery SFM model itself is very computation intensive.

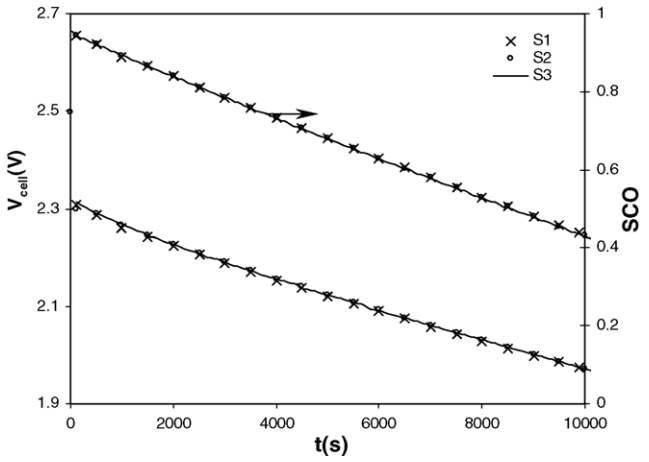


Fig. 8. Simulation run 1: Li-ion battery discharge with constant resistance load of 0.3 Ω. See Fig. 6 for the meaning of the legend.

Simulations of electrochemical cycling processes using battery models with CCVS interface are demonstrated in VTB environment (see Fig. 10). In the simulation, the batteries are charged and discharged through a current source which is controlled by a pulse signal generator.

The simulated cell voltage responses to the pulse current are presented in Figs. 11 and 12. As observed and expected, the cell voltage decreases in discharge and increases in charge. However, the first principle Li-ion battery model more accurately reflects the cell voltage responses than the simplified NiMH battery model does in the case of the relaxation phenomenon [13] which is shown in Fig. 12 right after the short term discharge and charge process as cell voltage slowly recovers even though no current flows in the circuit during those periods. The relaxation phenomenon is caused by the existence of the concentration gradient of lithium ions

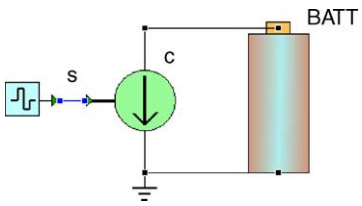


Fig. 10. Schematic of battery simulation.

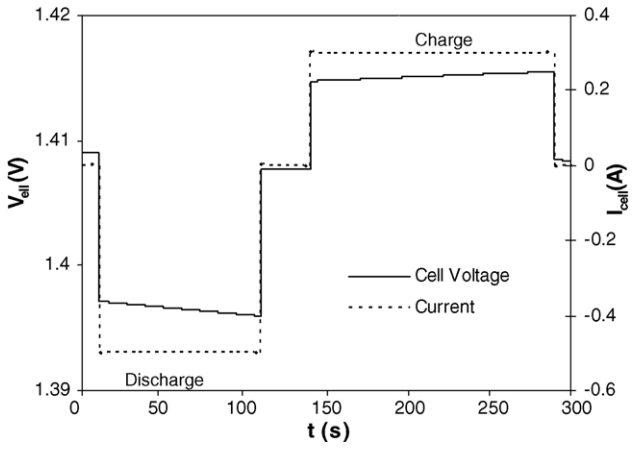


Fig. 11. Simulated NiMH cell voltage response to the pulse current.

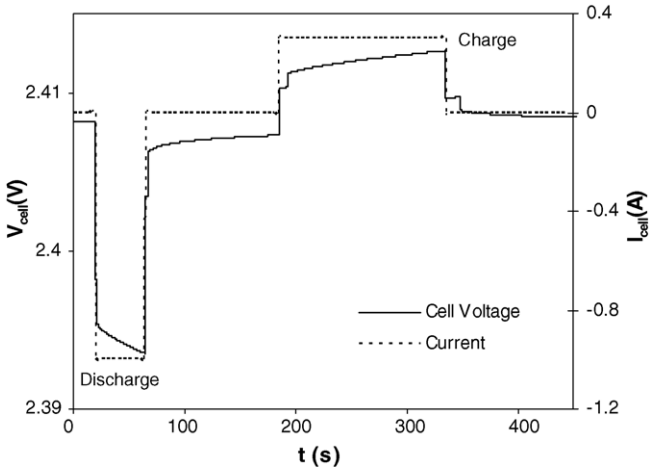


Fig. 12. Simulated Li-ion cell voltage response to the pulse current.

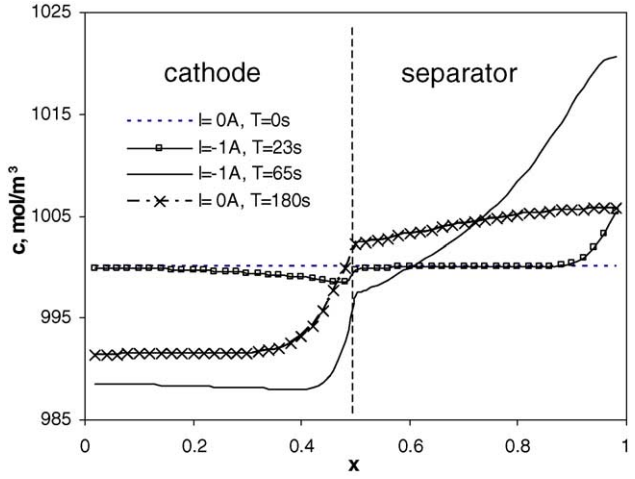


Fig. 13. Li-ion battery electrolyte concentration profiles in discharge and relaxation process of the Li-ion battery model. Dashed line divides the separator and composite cathode.

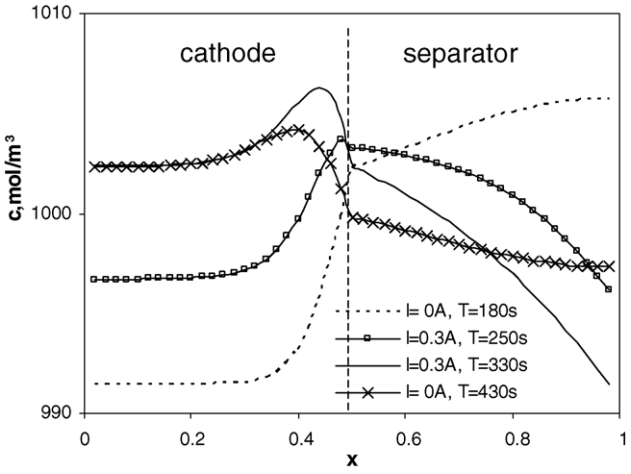


Fig. 14. Li-ion battery electrolyte concentration profiles in charge and relaxation process of the Li-ion battery model. Dashed line divides the separator and composite cathode.

in the electrode and electrolyte formed in the discharge process and charge process. Lithium ion concentration profiles in the battery are presented in Figs. 13 and 14 for the first current pulse. Driven by the concentration gradient, solution phase lithium ions at the electrolyte-electrode interface which are consumed or regenerated by the electrochemical reactions are replenished or dispersed through diffusion. Because no diffusion phenomenon is considered in the NiMH battery model, the relaxation behavior does not show up in the results as expected.

## 4. Conclusions

The resistive companion modeling of batteries with two electric type terminals is introduced in the paper. The methods can be generally applied to other physical type models such as mechanical or hydraulic ones so long as energy conservation equations are satisfied in the form of across and through variables. Native RC modeling method and the one using CCVS interface are presented in accordance to the complexity and computation requirement of battery models. It is conclude from our work that using CCVS interface is currently the first choice to model batteries in VTB. Simulations using RC models with CCVS interface are demonstrated on VTB platform and some results are presented and discussed. The ready availability of the VTB software and models of electric equipments make the VTB environment useful to study the design and performance of advanced power sources.

## Acknowledgment

The authors are grateful for the financial support of the project by the National Reconnaissance Office (NRO) under contract # NRO-000-03-C-0122.

## References

[1] J.S. Newman, Electrochemical Systems, 2nd ed., Prentice-Hall, NJ, 1991.
[2] Z. Jiang, R.A. Dougal, S. Liu, J. Power Sources 122 (2003) 95.
[3] V. Badescu, Energy 28 (2003) 1165.
[4] R.A. Dougal, S. Liu, L. Gao, M. Blackwelder, J. Power Sources 110 (2002) 285.
[5] T.E. Lovett, E.V. Solodovnik, Resistive Companion Modeling and Simulation for the Virtual Test Bed, Department of Electric Engineering, University of South Carolina, 2003.
[6] C. Alexander, M. Sadiku, Fundamentals of Electric Circuits, 1st ed., McGraw-Hill, NY, 1999.
[7] B. Wu, R. Dougal, R.E. White, J. Power Sources 93 (2001) 186.
[8] M. Doyle, T.F. Fuller, J. Newman, J. Electrochem. Soc. 140 (1993) 1526.
[9] V.R. Subramanian, J.A. Ritter, R.E. White, J. Electrochem. Soc. 148 (2001) E444.
[10] S. Li, L. Petzold, Design of new DASPK for sensitivity analysis, UCSB Technical Report, 1999.
[11] W. McKay, A. Monti, E. Santi, R. Dougal, A co-simulation approach for ACSL-based models, in: Proceedings of the Huntsville Simulation Conference, Huntsville, AL, 2001.
[12] Compaq Visual Fortran Programmer's Guide, Compaq Computer Cooperation, Texas, 2001.
[13] T.F. Fuller, M. Doyle, J. Newman, J. Electrochem. Soc. 141 (1994) 982.